Journal of the European Ceramic Society **19** (1999) 2519–2527

PII: S0955-2219(99)00116-8
0955-2219/99/$ - see front matter

Suitability of Mullite for High Temperature Applications

Ramón Torrecillas,[a]* José M. Calderón,[a] José S. Moya,[b] Michael J. Reece,[c] Craig K. L. Davies,[c] Christian Olagnon[d] and Gilbert Fantozzi[d]

[a]INCAR-CSIC, La Corredoria s/n Ap.73, 33080 Oviedo, Spain
[b]ICMM-CSIC, Cantoblanco, Madrid, Spain
[c]QMW College, Mile End Road, London E1 4NS, UK
[d]GEMPPM, INSA de Lyon, 69621 Villeurbanne Cedex, France

Abstract

High temperature mechanical behaviour of mullite has been studied. Our study include tensile, flexural and compressive creep behaviour and fracture up to 1400 °C. The results obtained in creep are analysed and compared with previous work in the literature. Two regions with different behaviour can be distinguished. The creep rates in bending, tension and compression are very similar in the first region at low stresses and temperatures. It is shown that in this region creep takes place by accommodated grain boundary sliding assisted by diffusion. At higher stresses slow crack growth from defects present in the sample occurs. The stress at which this transition in the deformation mechanism happens is dependent on several factors, the loading system during testing, the grain size, the amount and distribution of glassy phase and the environment. It is claimed the existence of a network of mullite–mullite grain boundaries free of glassy phase associated to the low surface energy of [001] planes. The diffusion rate through these boundaries controls the creep rate, and explains the high creep resistance of mullite. The results presented in this work lead to the conclusion that the mechanism controlling high temperature deformation resistance of mullite materials in a wide range of stress–temperature working conditions is independent of the glassy phase content. Slow crack growth limit the use of mullite at high stresses and temperatures. © *1999 Elsevier Science Ltd. All rights reserved.*

Keywords: grain boundaries, creep, fracture, mechanical properties, mullite.

*To whom correspondance should be addressed. Fax: + 34-98-529-7662; e-mail: rtorre@muniellos.incar.csic.es

1 Introduction

Mullite-based ceramics have been widely used as refractories and in pottery for many years. Mullite has good chemical stability and a stable temperature-independent oxygen vacancy structure [1] up to the melting point, low thermal expansion coefficient, $4{\cdot}5\times10^{-6}$ C^{-1}, low thermal conductivity, 0·06 W cm^{-1} K^{-1}, low dielectric constant, $\in\sim7$, high deformation resistance at high temperatures and low fracture toughness ($\sim$2 MPa $m^{1/2}$).[2–4]

Mullite did not appear as a stable phase in early phase equilibrium diagrams for the Al_2O_3–SiO_2 system. Bowen and Grieg in 1924 published the first phase diagram which included mullite, but did not determine a solid solution range.[5] It was not until 1954 that Shears and Archibald reported a solid solution region range from $3Al_2O_3{:}2SiO_2$ to $2Al_2O_3{:}SiO_2$.[6] In 1987 Klug published his version of the SiO_2–Al_2O_3 phase diagram showing the shifting of the mullite solid solution region towards higher Al_2O_3 contents at temperatures higher than the eutectic point (1587 °C).[7] This shifting results in the presence of a silica-rich glassy phase for a 3:2 mullite sintered at temperatures higher than the eutectic. In order to obtain mullite monolithic materials free of glassy phase two routes can be used. One method is to use mullite powders obtained by the sol–gel method crystallised at high temperature, around 1200 °C, and sintered at temperatures well below the eutectic. Nixon hot pressed highly pure mullite below 1300 °C using this method.[8] The other method is to use mullite with a higher alumina content that can be sintered at higher temperatures remaining in the solid solution region.

Most of the work in the literature uses 3:2 mullite sintered at temperatures between 1600 and 1700 °C, and as a consequence has a remaining glassy phase in the microstructure.

Concerning the mechanical properties, the availability of fine pure mullite powders and new

processing routes have made it possible to obtain dense polycrystalline mullite with higher deformation resistance at higher temperatures than most other ceramics, i.e. alumina.[9] Although there is already some work done in tensile creep,[10] the majority of studies on high temperature mechanical properties of mullite have concentrated on measurements of the strength or the creep deformation under testing conditions of four point bending or compression under static loading. These testing procedures are useful as an initial evaluation of failure strength or creep resistance but the complexity of the stress makes it difficult to interpret the effect of the material variables on the creep mechanisms.

This work introduces creep results obtained in four-point bending, compression and tension on the same mullite material.[11–13] The material chosen is a commercial 3:2 mullite. The aim of the study was to analyse the creep of mullite using different testing methods and to explain the effect of the test method on creep behaviour of the different loading states on the samples in a wide range of stresses and temperatures. Microstructural features were considered in order to determine the dominant creep mechanisms in the experimental ranges of stresses and temperatures studied. Our results are compared with previous data in the literature.

2 Experimental

A commercial mullite powder (Baikowski 193 CR, France) with an average particle size of 2·7 μm and a specific surface of 3·1 $m^2 g^{-1}$ was used. The X-ray diffraction pattern indicates that the powder is predominantly mullite with possible traces of cristobalite and corundum. A molar ratio $Al_2O_3/SiO_2 = 1{\cdot}62$ was determined by chemical analysis. This powder was prepared for subsequent processing by spray drying a slurry to a particle agglomerate size of 80 μm. The water based slurry contained additives to act as a lubricant and a binder, together with a dispersing agent and an agent to reduce gas bubble formation. The spray dried mullite powder was cold isostatic pressed at 200 MPa into plates and rods, green machined, sintered at 1750 °C–5 h and then annealed at 1450 °C for 5 h in order to promote the crystallisation of the amorphous glassy phase present at the sintering temperature. Finally the different samples for mechanical testing were machined from sintered bars and blocks. The real density and the apparent density of the fired samples were found to be 3·037 and 2·948 g cm^{-3}, and the calculated porosity was found to be 2·94%.

Parallelepipeds of dimensions 4×3×40 mm were tested in four-point bending with an inner and outer span equal to 18 and 36 mm, respectively. In any cases the tensile face of the specimens was polished to 3 μm. A constant load, P, was applied during creep testing on the loading points and the maximum vertical deflection was recorded on the tensile face of the specimen halfway between the loading points. A load cell on the device allowed us to show that the frictional forces remained negligible during loading. A detailed description of the measurement technique and creep apparatus is given elsewhere.[14] The analysis of creep have assumed that for small strains the stress can be calculated using the standard linear elastic formula:

$$\sigma = 3P(s_2 - s_1)/2BW^2, \tag{1}$$

where P is the applied load, B is the breadth, W the depth of the sample and s_2 and s_1 the outer and inner spans, respectively. The strain is calculated assuming that the strain rate, ε', and the stress, σ, are related by

$$\varepsilon' = D\sigma^n, \tag{2}$$

where D and the stress exponent, n, are constants. Hollenberg *et al.*[15] showed that if there is no major cracking in the specimen and the creep rates in tension and in compression are similar the maximum strain, ε, and deflection, y_c, are related by

$$\varepsilon = 2W(n+2)/\{(s_2 - s_1)[s_2 - s_1(n+1)] + s_2^2(n+2)/2\}y_c. \tag{3}$$

The specimens for tensile testing were cylindrical rods of 150 mm length, 9·00 ± 0·01 mm maximum diameter on the edges, with a gauge length of 20 mm in the centre with a diameter of 5·00 ± 0·01 mm. A good alignment was achieved, with < 5% of bending stress on the samples at specimen failure. All specimens were strain gauged and the room temperature bending checked prior to testing. The specimen strain was measured with either an external or a side entry extensometer attached to the specimen gauge length, and to capacitance transducers. Details of the testing rigs used can be found elsewhere.[14]

Parallelepipeds of dimensions 2×2×4 were tested in compression. All surfaces were well aligned and polished down to 3 μm prior to testing to remove surface damage introduced by machining.

3 Results and Discussion

3.1 Microstructure

The resulting material presents both equiaxed and elongated grains with an aspect ratio ranging from 4 to 8 (Fig. 1), with an average grain size, d, of 4·0 μm.

The images obtained by transmission electron microscopy show the presence of an intergranular glassy phase located at triple points and some grain boundaries. Figure 2 shows a triple point filled with glass adjacent to a nonwetted boundary. The chemical composition of this glassy phase was determined by energy dispersive X-ray spectroscopy (EDX) analysis of different samples in the transmission electron microscope, and was found to be $13 \pm 1{\cdot}6$ mol% of Al_2O_3 and $87 \pm 1{\cdot}6$ mol% SiO_2. This is a high viscosity silica-rich glassy phase.

Other regions are characterised by the presence of clean grain boundaries. These observations are consistent with the results of Kleebe,[16] who found that depending on the orientation of the mullite grains, wetted and nonwetted grain boundaries coexisted. It seems that low energy grain boundaries that are not wetted by the silica rich glassy phase are always present in monolithic mullite materials.

3.2 Mechanical results

The creep behaviour of the mullite material at 1400 °C is shown in Fig. 3 in a logarithmic strain rate versus stress plot. Figure 4 shows the behaviour in bending at different temperatures. In these plots stationary states of deformation for different stresses and temperatures are represented, so the stress exponent, n, can be determined. The stationary strain rates are obtained from the strain versus time plots when the slope of each curve reach a constant value, for each stress and temperature. We can discriminate between two regions with different values of the stress exponent, noted n_1 and n_2 in Fig. 4. The region of lower stresses, n_1, is characterised by a constant value of the stress exponent, $n_1 \sim 1$, and the creep rates are very similar for the three testing procedures. The n value diverges in the high stresses region (n_2). This acceleration of creep is observed in tension at lower stresses than in compression. The change in the slope is due to the appearance of slow crack growth, as we will justify later. Tensile testing may ease the opening of grain boundaries as well as the creation of cavities and cracks compared to compressive loading.

In order to make a complete characterisation of creep behaviour the bending test was selected. Figure 4 presents results in a logarithmic strain rate versus stress plot for the range of temperatures studied, from 1100 to 1450 °C. We can discriminate between two regions: the low stresses region, with values of n_1 close to 1, and the high stresses region,

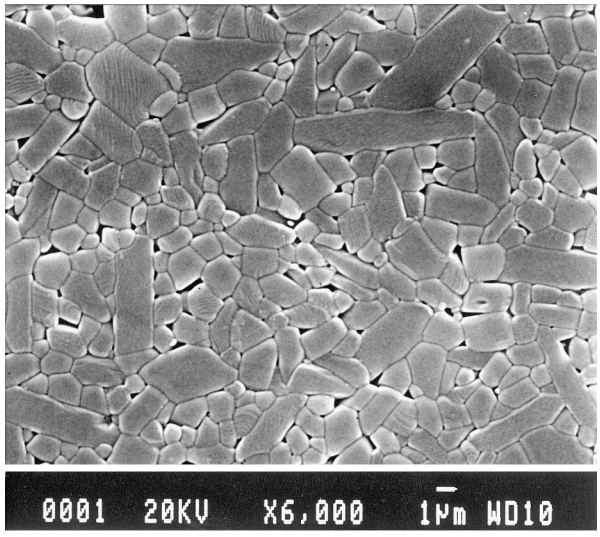

Fig. 1. SEM micrograph of a thermally etched surface showing the grain size and the presence of elongated grains.

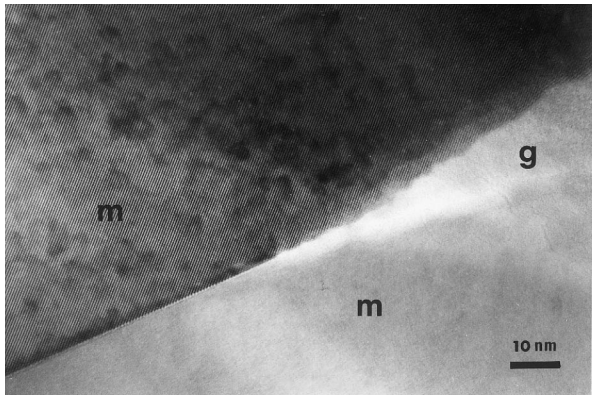

Fig. 2. TEM micrograph, showing a glassy (G) pocket at a triple point, and an adjacent nonwetted boundary between two mullite (M) grains.

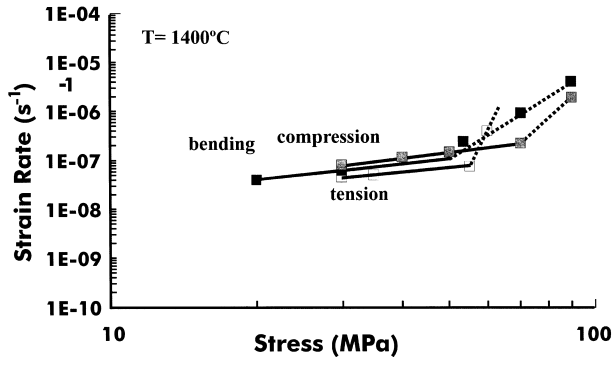

Fig. 3. Creep rates at 1400°C for different testing methods.

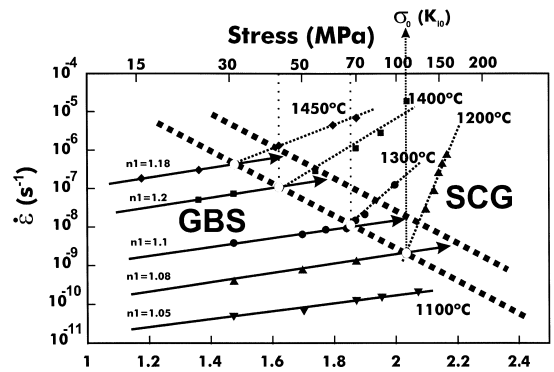

Fig. 4. Logarithmic *strain rate* versus *stress* plot, showing the creep behaviour in bending at different temperatures.

where the stress exponents increase with stress to higher values between 3 and 19, these apparent stress exponents are labelled n_2 in the figure and cannot be considered as true stress exponents. This behaviour can be explained taking into account that in the range of high stresses the apparent stress exponent value is calculated from strain rates close to the moment of fracture and the value is overestimated. The overestimation of strain rates at higher stresses becomes clear when we represent the evolution of strain rate versus time of the samples deformed in this high stress region (Fig. 5). It can be observed that fracture occurs during primary creep, before a truly stationary state could be observed. In these cases the values determined for the stress exponents do not have the same significance as in the low stress region.

The stresses defining the limit between the regions with n_1 and n_2 values for different temperatures draw a straight line in Fig. 4, represented as a dotted line.

The activation energies have been determined in a log ε' versus $1/T$ plot. Figure 6 shows the results obtained for three different stresses, 30, 50 and 70 MPa. The curves show two different slopes for a given stress. At lower temperatures the activation energy is $Q = 410\,\text{kJ mol}^{-1}$ for all the stresses. At higher temperatures, above 1300 °C, the activation energy increases with stress, to 731 and 930 kJ mol^{-1} at 30 and 70 MPa, respectively. The same considerations applied to the n values in this region can be applied to these increasing Q values. The strain rates measured to determine the Q values do not correspond to true stationary states of creep and they do not have their usual meaning as parameters of stationary creep given by the classical creep equation (4).

The microstructural characterisation by SEM of the deformed samples shows that in the region of higher stresses fracture occurs first by intergranular propagation of defects until they reach a critical size causing the fracture of the sample in a transgranular manner. Figure 7 shows the transition between these two regions.

In the case of samples deformed at low stress, the microstructure of tensile surfaces does not change even at high deformation levels. Figure 8 shows a tensile surface deformed to a 2·1% without creep damage. The microstructural observations of crept samples in this region do not agree with any creep mechanism that requires cavitation or opening of grain boundaries.

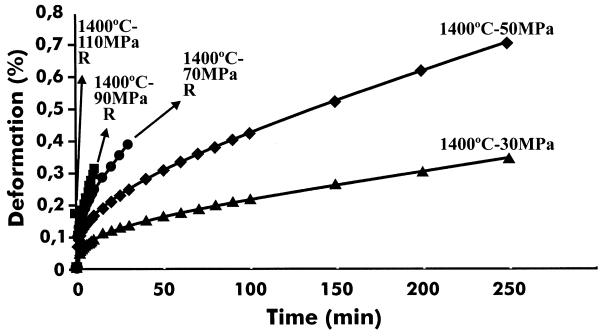

Fig. 5. *Strain rate* versus *time* plot, showing the moment of fracture for each stress at 1400°C.

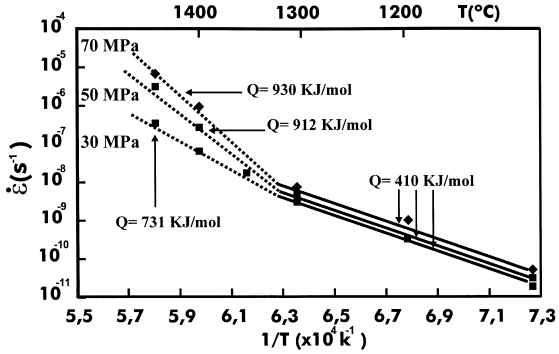

Fig. 6. Log (*strain rate*) versus $1/T$ plot for different stresses, showing the values of Q determined from the curves. In some cases this quantitative value has no meaning, does not represent any activation energy.

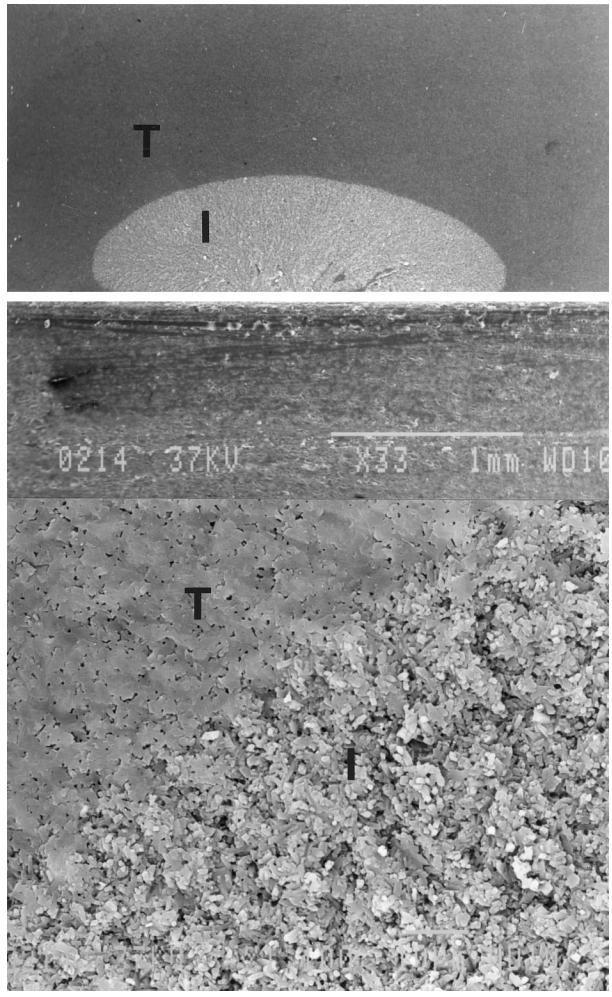

Fig. 7. Fractured surface showing the slow crack growth region, where defects propagate intergranularly until they reach a critical size, and the region of fast crack growth and transgranular fracture and micrograph at higher magnification of the transition between the intergranular fracture region (I) and the transgranular fracture region (T).

In the testing temperature range between 1200 and 1500 °C several authors have determined the creep parameters of the eqn (1) for different mullites.

$$\varepsilon' \propto \sigma^n d^{-p} e^{--Q/kT} \tag{4}$$

where p is the grain size exponent, Q is the activation energy, and kT has its usual meaning.[17–23] They have found values for the activation energies ranged from below 360 kJ mol^{-1} to more than 1000 kJ mol^{-1}, while the stress exponent and the grain size exponent had values between 1 and 2, and between 2 and 3, respectively. Creep rates differs by orders of magnitude for different dense monolithic mullite ceramics at the same temperature. Studies of creep from different laboratories can lead to a significant scatter in results due to small differences in composition, microstructure and processing, and to the use of different testing procedures.

In Fig. 9 we have compared the results of this work with the behaviour of other mullite materials processed by different methods, with different contents in glassy phase and grain sizes from 1 to 4 μm, and tested in compression and four-point bending. It can be observed (Fig. 9) that the experimental creep rates are widely scattered, within a factor of nearly three orders of magnitude.

A great part of the scatter can be explained if we consider the dependence of the strain rate with the grain size. Grain boundary sliding accommodated by diffusion will result in a grain size exponent, p, in eqn (1) between 2 and 3, depending on the diffusion path, $p=2$ when the diffusion takes place through the volume of the grain, and $p=3$ when the diffusion takes place in the grain boundaries.[24–26] We have normalised the results in the figure using $p=2$, and $p=3$, in the stress and temperature ranges corresponding to the true stationary creep. In this region no slow crack growth has been observed, the curves at different temperatures in a logarithmic strain rate versus stress representation are parallel, and the values of the activation energy can be determined with a proper meaning. The results of normalisation are shown in Figs. 10 and 11. It can be observed that the scatter of results is reduced very significantly to a factor between 4 and 5 when considering the normalised rates $\varepsilon \times d^2$, and also between 4 and 5 when using $\varepsilon \times d^3$.

The results of the normalisation means that: (i) the mechanism or mechanisms controlling creep have the same dependence with grain size in all the mullite materials processed and tested by different methods; (ii) the mechanism is probably the same in all the materials. The latter assumption can be

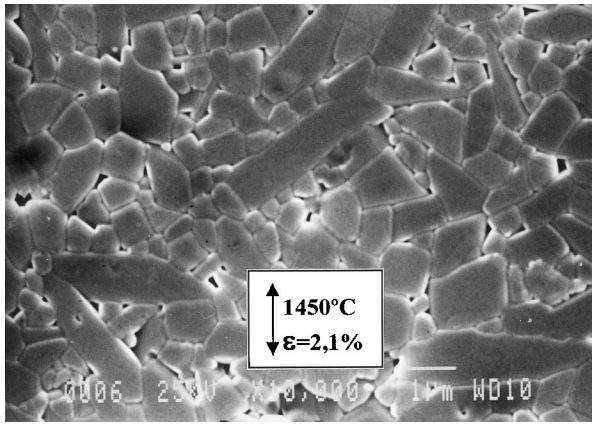

Fig. 8. Microstructure of a sample deformed in the low stresses region. In this region the creep takes place by accommodated sliding of the grains, and no changes can be observed after the deformation.

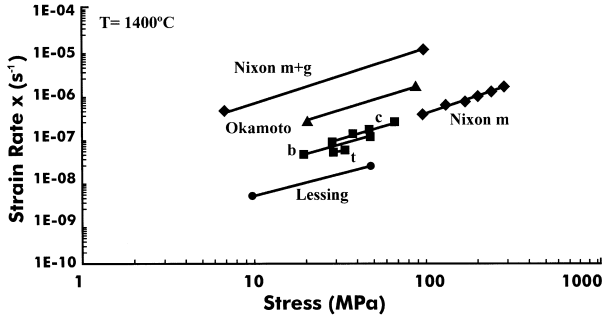

Fig. 9. Logarithmic *strain rate* versus *stress* plot, showing the creep behaviour of different mullite materials. The shadowed area represents the maximum scattering of creep rates.

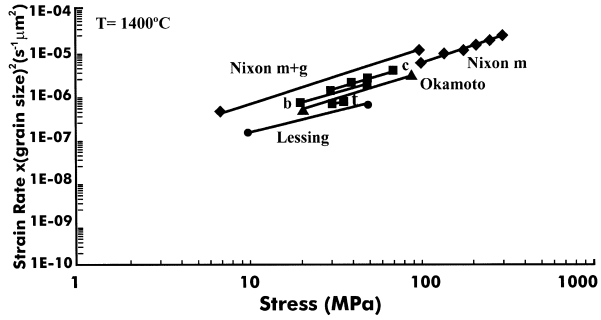

Fig. 10. Logarithmic *normalised strain rate* versus *stress* plots, creep rates are normalised with the grain size using a grain size exponent $d=2$. The shadowed area represents the maximum scattering of creep rates.

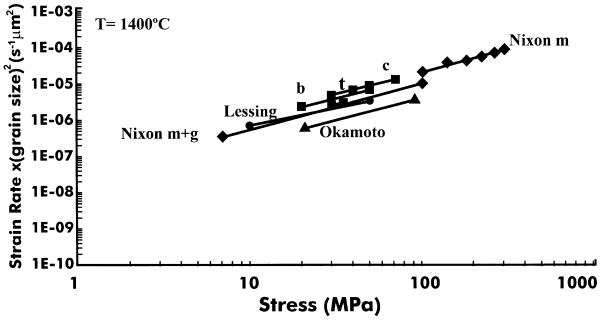

Fig. 11. Logarithmic *normalised strain rate* versus *stress* plots, creep rates are normalised with the grain size, using a grain size exponent $d=3$. The shadowed area represents the maximum scattering of creep rates.

justified by two facts: first in the range of stresses and temperatures the curves have the same slope, that is, the same n value, and second the matching of the normalised creep curves for different materials. The creep rates after normalisation converge towards one only creep curve (Figs 10 and 11). The scatter observed in normalised creep rates is very low, and has been greatly reduced from the experimental data. Since we are comparing materials processed by different routes, there are small differences in sample composition; in micro-structural features such as porosity, in the aspect ratio of grains, in the grain size and the grain size distribution, and in the amount of glassy phase and distribution thorough the sample. Different testing methods at different laboratories will introduce additional experimental scatter. All these factors together are likely to cause a wider scatter that is not observed after the normalisation. It seems that the mechanism controlling the creep rates in all the materials is not significantly dependent of other processing variables apart from the observed dependence with grain size.

The amount of glassy phase, usually considered of great importance in determining the creep resistance, is believed to be responsible for big differences in strain rates found between different mullite ceramics.[8,18,19] However, we think that the absence of glassy phase may have another effect than dramatically lowering the creep rate. There is a limit in the stress and strain rate that a particular mullite ceramic can stand deforming by stationary creep, this critical value is probably affected significantly by several parameters, one of which is the amount of glassy phases present. The degradation of the material through the opening of pores can be eased by the presence of substantial amounts of glassy phases, particularly when the sample is subjected to tensile loading.

Nixon studied creep of two mullite ceramics with and without glassy phase.[8] He found creep rates for the glass free material were nearly two orders of magnitude lower. Once taken into account the different grain sizes, the normalised creep rates are very similar, but stationary creep is observed at much higher stresses, up to 300 MPa, for the glass free mullite (Fig. 11).

Hynes compared the creep of one pure mullite and one mullite with 6 wt% glassy phase with similar grain sizes.[18] The sintering temperature was higher than the eutectic temperature for both materials. The method used to avoid the formation of glass was to increase the alumina content, moving in the phase diagram towards the liquid free region for the processing temperature. It is possible that there was some alumina present at the grain boundaries. No direct measurement of the glass present was made. A significant difference in the creep rates was found, but not enough to justify a dependence of creep rates with the third power of glassy phase volume fraction, as it is predicted by models based on the viscous flow of mullite hard grains on amorphous silica. Because of the observed microstructural evolution and the values obtained for creep parameters the authors suggested that the same mechanism was rate controlling the creep for both materials. The activation energies were determined in the high stress region and the values founded were high (>700 kJ mol^{-1}). The stress exponent for the mullite containing glass was somewhat high, $n=1{\cdot}6$, and $1{\cdot}2$ for the pure mullite. At low stresses the strain rates are closer.

The convergence of strain rates at lower stresses agrees with our view that a higher content of glassy phases reduces the critical stresses at which slow crack growth appears and the creep accelerates. Further study with a careful control of the amount of glass present at the grain boundaries in different mullite ceramics is necessary to avoid controversy on this point.

Given the very good agreement of normalised creep rates in the lower stress region, the wide range of activation energies determined by different authors is not understood. Higher values are obtained at higher temperatures (Fig. 6). However, these values are often obtained outside the region of low stresses, or at least partially the stresses used for the determination of Q at different temperatures are situated above the critical stresses of appearance of slow crack growth for the highest temperature or temperatures used. High apparent Q values measured are due to the creation of some creep damage during testing.

Creep rates will be controlled by the slower accommodating mechanism. At high temperatures, where creep can be observed, self-diffusion of mullite will be slower than the transport of matter by solution-precipitation of mullite in the silica-rich glassy phase, and the Q values should be those of the slowest mechanism controlling the creep rate. The discrepancy in the values requires a correct evaluation of all diffusional paths in polycrystalline mullite.

Work by Mizuno,[27] and later by Kleebe,[16] has shown an important feature of the microstructure of monolithic mullite. This is the accumulation of glassy phases in triple points, and the absence of glassy films in all or certain type of boundaries, depending of the crystallographic orientation of the grains. Mizuno observed by high resolution transmission electron microscopy that no glassy phases were present in any observed grain boundary, despite the sintering at a temperature well

above the eutectic point, where liquid is a stable phase in the SiO_2–Al_2O_3 diagram. He observed the presence of glass only as amorphous pockets at triple points. Kleebe observed that boundaries including a [001] plane are clean of an amorphous thin layer. High resolution TEM showed total absence of a glassy film, but electron energy loss spectroscopy (EELS) showed wetted and clean boundaries. This inhomogeneity in the distribution of glassy phases had not been reported before in mullite.

The fact that there are clean grain boundaries explains why creep in mullite requires the activation of self–diffusion. In the interfaces mullite–mullite free of glassy phase there is no other option to accommodate creep. If there is no diffusion at the glassy free mullite-mullite boundaries interlocking of mullite grains will impede grain boundary sliding. Deformation will be stopped until the local stress intensity factor reached the critical value and cause the propagation of a crack.

Different stationary creep mechanisms, Nabarro–Herring,[24,25] Coble,[26] flow of hard grains in a viscous phase, suggested by Hynes[18] following the model by Dryden,[28] or solution–precipitation[29] of mullite in the presence of a viscous phase, have been proposed for mullite.[8,9,12,17–23] Of these, flow of hard grains in a viscous phase and solution-precipitation require the presence of a continuous glassy film in the grain boundaries. However experimental evidence have demonstrated that certain crystallographic planes of mullite grains appear always clean of glassy phases. Therefore, we have to eliminate these mechanisms as responsible for the control of creep, although some contribution may be expected in wetted boundaries with glass.

Nabarro–Herring, Coble mechanisms, or diffusionally accommodating grain boundary sliding as described by Lifshitz[30] or Ashby–Verrall[31] predict stress exponents close to 1 and grain size exponents between 2 and 3. At the interfaces clean of glassy phase, we can consider the overall contribution of Nabarro–Herring, Coble creep and grain boundary sliding with one equation. Pure diffusion predicts a creep rate[32]

$$\varepsilon' = 14\sigma\Omega/kTd^2D_{\mathrm{ef}}, \tag{5}$$

where Ω is the atomic volume of diffused species, d is the grain size, σ is the stress, and D_{ef} is

$$D_{ef} = \left(D_v + \pi\delta D_{\mathrm{gb}}/d\right), \tag{6}$$

where D_{v} and D_{gb} are the coefficients of diffusion in volume and in the grain boundaries, respectively, and δ is the grain boundary width. Accommodated grain boundary sliding models require diffusion for the transport of matter in those grain boundaries deviated from perfect planes where due to sliding a local stress field is generated. Without the relaxation of the stresses the grain boundary sliding would be stopped until the creation of cracks. For a polycrystal with equiaxed grains and high strains the dependence with stress and grain size is the same as in pure diffusional creep, but strain rates would be higher by a factor of 7.[33] For example in the Ashby–Verrall model eqn (2) becomes

$$\varepsilon' = 98(\sigma - \sigma_u)\Omega/kTd^2D_{\mathrm{ef}} \tag{7}$$

where D_{ef} has the same meaning that in (2), and σ_{u} is the threshold stress needed to activate grain boundary sliding. For high stresses the dependence with the stress is the same, but accommodated grain boundary sliding predicts higher strain rates and therefore will be the dominant creep mechanism.

Mullite materials with very different origins and tested in different laboratories have shown the same dependence with grain size and stress, and the normalised creep rates become very close, as can be seen in Figs 10 and 11. Therefore, we assume that in the region of stationary states considered there is only one common mechanism controlling the creep rates in all the materials. We believe that the dominant creep mechanism is diffusionally accommodated grain boundary sliding.

In order to have an experimental evidence of the slow crack growth appearance at high stresses and temperatures, the crack velocity versus stress intensity factor behaviour have been determined using the double torsion technique. A detailed description of this study can be found in a former work.[34] A threshold stress intensity factor, K_{I0}, of 1·6 MPa $m^{1/2}$ was found, no slow crack growth is observed for stress intensity factors below this value.

An approximate size of pre-existent flaws in the material can be calculated from values of the fracture strength, σ_{f}, and the fracture toughness, K_{Ic}, using the Griffith theory. The fracture strength was determined in bending and the fracture toughness by the single edge notched beam technique. A detailed description of the results can be found elsewhere.[34]

The stress required to initiate slow crack growth in the material, σ_{SCG}, can then be obtained approximately from the ratio $\sigma_{\mathrm{f}}/K_{\mathrm{Ic}}$ and the K_{I0} values determined by double torsion, with the following equation:

$$\sigma_{\mathrm{SCG}} = (\sigma_{\mathrm{f}}/K_{\mathrm{Ic}})K_{\mathrm{I0}} \tag{8}$$

The results are given in Table 1. We have compared in Table 1 the values of σ_{SCG} to the stress

Table 1. Values of K_{Ic}, σ_f, K_{I0}, σ_{SCG} and σ_t at different temperatures. σ_{SCG} values are obtained from K_{Ic}, σ_f, K_{I0} values[34] and σ_t from Fig. 4

T (°C)	K_{Ic} (Mpa $m^{1/2}$)	σ_f (MPa)	K_{I0} (Mpa $m^{1/2}$)	σ_{SCG} (MPa)	σ_t (MPa)
1200	3·6 ± 0·1	260 ± 15	1·6 ± 0·1	115 ± 17	105
1300	3·5 ± 0·2	200 ± 20	1·6 ± 0·1	91 ± 20	71
1400	3·3 ± 0·2	120 ± 25	1·6 ± 0·1	58 ± 18	45

values, noted as σ_t , which define the limits between n_1 and n_2 regions defined in Fig. 4. We consider that in the n_1 region deformation takes place by accommodated grain boundary sliding creep and in the n_2 slow crack growth appears. Values of σ_{SCG} not only follow the same trend with temperature, the values are in good agreement with the stresses defining the transition to the n_2 region. The results thus confirm our assumption that the different behaviour in the high stress and temperature region correspond to the activation of slow crack growth.

The region at which accommodated grain boundary sliding controls creep is limited to a maximum stress and strain rate for each temperature (Fig. 4). We can define pairs of critical values (critical strain rate, critical stress) that will determine the limit between the region of creep characterised by uniform values of stress exponent and activation energy, and the region characterised by the growth of cracks and accelerated creep rates. We can call the latter one the sub-critical crack growth region. There is a wide region of temperatures and stresses in which mullite can work showing optimum creep behaviour, with very low strain rates. Above a certain stress for each temperature slow crack growth will appear, with the associated risk of catastrophic failure in a brittle manner.

To avoid the risk of catastrophic failure of mullite components in operation at high temperature we need to determine the range of stresses and temperatures at which deformation happens by accommodated creep and not by creep-damage or slow crack growth. The line separating both regions in the logarithmic ε'–σ plot will move towards the region of higher or lower stresses as a function of several parameters: state of stresses, grain size, presence and distribution of glassy phases and atmosphere.

The dependence with these parameters has to be studied to understand the creep of mullite as a monolithic material or as a matrix in mullite based composites.

4 Conclusions

4.1 High temperature mechanical behaviour

The creep behaviour of a monolithic mullite has been studied by different testing methods and compared with previous results for other mullite materials.

Previously it was known the excellent resistance of mullite under compressive loading. In this work mullite has shown the same creep resistance in tension and compression at low stresses. This fact supports the use of the Hollenberg model for the calculation of bending creep rates. Calculated bending creep rates are very similar than those obtained in tension and compression.

Creep rates have been normalised following a dependence with grain size $\varepsilon' \propto d^{-p}$, with $p = 2$ or $p = 3$, predicted by the accommodating creep mechanism. The scatter in strain rates narrows very significantly after the normalisation, with all materials close within a factor of 4.

It makes no sense to try the normalisation with grain size where the log ε'–log σ curves are not parallel, crack growth takes place and no proper parameters of creep can be obtained, i.e. the apparent activation energy values determined in this region change with the stress.

The creep mechanism in the low stress region is accommodated grain boundary sliding. Diffusion by stress-induced solution–precipitation, viscous flow of the grains in amorphous phase-rich zones and self-diffusion of mullite can all make some contribution to the strain during creep. The dominant accommodating mechanism is diffusional, most likely by grain boundary diffusion of mullite as the path controlling the creep rate. The possible inhibition of grain boundary sliding and deformation by pure diffusion creep in glass-free mullite will result in different creep rates after normalisation. This is not observed.

4.2 Suitability of mullite for high temperature applications

The suitability of mullite for high temperature applications in a wide range of temperatures and stresses has been demonstrated. In the region where crack growth is not observed catastrophic failure in a brittle manner does not occur. The limit between both regions defines a critical stress and strain rate, separating the region of extended creep from the slow crack growth region at each temperature. This stress should be the maximum operating stress to avoid risk of catastrophic brittle failure. This stress depends on the loading system applied on the sample, microstructural and environmental variables.

It has to be taken into account that the use of tensile stresses will shift the slow crack growth region to lower stresses. The absence of glassy phase seems to increase the critical stresses, allowing the use of structural mullite components at higher stresses. Mullites with higher alumina contents could avoid the formation of liquid during sintering and consequently could extend the safety margin to higher stresses and temperatures without the risk of slow crack growth and catastrophic brittle failure.

Studies of fracture and fatigue on mullite will help to understand the appearance of slow crack growth to extend the suitable range of stresses and temperatures for high temperature applications. For example, from results in crack growth studies, it is known that low levels of humidity reduce the crack growth rates.[35] It is possible that this effect also appears in creep, and at low humidity testing environment slow crack growth will appear at higher stresses. We intend to continue the present work studying the effect of other variables, as the testing environment, on mullite creep.

Acknowledgements

This work was supported by the Brite EuRam III Project BRE2CT94 0613.

References

1. Paulmann, C., Study of oxygen vacancy ordering in mullite at high temperature. *Phase Transitions*, 1996, **59**, 77–90.
2. Scnneider, H., Okada, K. and Pask, J., *Mullite and Mullite Ceramics*. John Wiley and Sons, Chichester, 1994.
3. Somiya, S., Davis, R. F. and Pask, J. A., Mullite and mullite matrix composites. Ceramic Transactions, Vol. 6, Proceedings of the Int. Conf. on Mullite, Tokyo, November 1987.
4. Aksay, I. A., Dabbs, D. M. and Sarikaya, M., Mullite for structural, electronic, and optical applications. *J. Am. Ceram. Soc.*, 1991, **74**, 2343–2358.
5. Bowen, N. L. and Grieg, J. W., The system Al_2O_3–SiO_2. *J. Am. Ceram. Soc.*, 1924, **7**, 238–254.
6. Shears E. C. and Archibald W. A., Aluminosilicate refractories. *Iron Steel*, 1954, **27**, 26–30, 61–65.
7. Klug, F. J., Prochazka, S. and Doremus, R. H., Alumina-silica phase diagram in the mullite region. *J. Am. Ceram. Soc.*, 1987, **70**, 750–759.
8. Nixon, R. D., Chevacharoenkul, S. and Davis, R. F., Creep of hot-pressed SiC-whisker-reinforced mullite. *Ceram. Trans.*, 1990, **6**, 579–603.
9. Lessing, P. A., Gordon, R. S. and Mazdiyasni, K. S., Creep of polycrystalline mullite. *J. Am. Ceram. Soc.*, 1975, **58**(3–4), 149–150.
10. Kumazawa, T., Ohta, S., Tabata, H. and Kanzaki, S., Influence of chemical composition on the mechanical properties of SiO_2–Al_2O_3 ceramics. *J. Ceram. Soc. Jpn.*, 1988, **96**, 85–91.
11. Rhanim, H., Olagnon, C., Fantozzi, G. and Torrecillas, R., Crack propagation behaviour in mullite at high temperature by the double-torsion technique. *J. Eur. Ceram. Soc.*, 1997, **17**, 85–89.
12. Calderon-Moreno, J. M. and Torrecilas, R., High temperature creep of polycrystalline mullite. *Key Eng. Mat.*, 1997, **132–136**, 587–590.
13. Torrecillas, R., Fantozzi, G., de Aza, S. and Moya, J. S., Thermomechanical behaviour of mullite. *Acta Mater.*, 1997, **45**(3), 897–906.
14. Davies, C. K. L., Reece, M. J., Torrecillas, R. and Fantozzi, G., Development of High Temperature Fatigue, Creep and Thermal Shock Resistant Zircon and Mullite-Zirconia Ceramics. Final technical report. Brite-EuRam III Contract BR2-CT94-0613, Project BE-8058, 1998.
15. Hollenberg, G. W., Terwillinger, G. R. and Gordon, R. S., Calculation of stresses and strains in four-point bending creep tests. *J. Am. Ceram. Soc.*, 1971, **54**(4), 196–199.
16. Kleebe, H. J., Hilz, G. and Ziegler, G., Transmission Electron Microscopy and Electron Energy Loss Spectroscopy characterization of glass phase in sol-gel derived mullite. *J. Am. Ceram. Soc.*, 1996, **79**(10), 2592–2600.
17. Okamoto, Y., Fukudome, H., Hayashi, K. and Nishikawa, T., Creep deformation of polycrystalline mullite. *J. Eur. Ceram. Soc.*, 1990, **6**, 161–168.
18. Hynes, A. P. and Doremus, R. H., High temperature compressive creep of polycrystalline mullite. *J. Am. Ceram. Soc.*, 1991, **74**(10), 2469–2475.
19. Ohira, H., Shiga, H., Ismail, M. G. M. U., Nakai, Z. and Akiba, T., Compressive creep of mullite ceramics. *J. Mat. Sci. Lett.*, 1991, **10**, 847–849.
20. Ohnishi, H., Maeda, K., Nakamura, T. and Kawanami, T., High temperature mechanical properties of mullite Ceramics. *Ceram. Trans.*, 1990, **6**, 605–612.
21. Hiroshi Ohnishi Kawanami, T., Nakahira, A. and Niihara, K., Microstructure and mechanical properties of mullite ceramics. *J. Ceram. Soc. Jpn.*, 1990, **98**(6), 541–547.
22. Dokko, P. C., Pask, J. A. and Mazdiyasni, K. S., High temperature mechanical properties of mullite under compression. *J. Am. Ceram. Soc.*, 1997, **60**(3–4), 150–155.
23. Ashizuka, M., Honda, T., Yoshitaka, Y. and Kubota, K., Effect of grain size on creep in mullite ceramics. *J. Ceram. Soc. Jpn.*, 1991, **99**(4), 292–295.
24. Nabarro, F. R. N., Steady state diffusional creep. *Phil. Mag.*, 1967, **16**, 231–237.
25. Herring, C., Diffusional viscosity of a polycrystalline solid. *J. Appl. Phys.*, 1950, **21**(5), 437–445.
26. Coble, R. L., A model for boundary diffusion controlled creep in polycrystalline materials. *J. Appl. Phys.*, 1963, **34**(6), 1679–1682.
27. Mizuno, M., Microstructure, microchemistry, and flexural strength of mullite ceramics. *J. Am. Ceram. Soc.*, 1991, **74**, 3017–3022.
28. Dryden, J. R., Kucerovsky, D., Wilkinson, D. S. and Watt, D. F., Creep deformation due to a viscous grain boundary phase. *Acta Metall.*, 1989, **37**(7), 2007–2015.
29. Raj, R., Tsai, R. L., Wang, J. G. and Chyung, C. K., Superplastic flow in ceramics enhanced by a liquid phase. In *Deformation of Ceramic Materials II*, ed. R. E. Tressler and R. C. Bradt. Plenum Press, New York, 1984, pp. 353–378.
30. Lifshitz, I. M., On the theory of diffusion-viscous flow of polycrystalline bodies. *Sov. Phys.*, 1963, **17**, 909.
31. Ashby M. F. and Verrall R. A., Diffusion accommodated flow and superplasticity. *Acta Metall.*, 1973, **21**, 149–163.
32. Cannon, R. M. and Coble, R. L., Review of diffusional creep of Al_2O_3. In *Deformation of Ceramic Materials*, ed. R. C. Bradt and R. E. Tressler. Plenum Press, New York, 1974, pp. 61–100.
33. Cannon, W. R. and Landon, T. G., Review creep of ceramics. *J. Mater. Sci.*, 1988, **23**, 1–20.
34. Davies, C. K. L., Reece, M. J., Torrecillas, R. and Fantozzi, G., Development of High Temperature Fatigue, Creep and Thermal Shock Resistant Zircon and Mullite-Zirconia Ceramics. Final report. Brite-Euram III project BR2-CT94-0613.
35. Davies, C. K. L., Guiu, F., Li, M., Reece, M. J. and Torrecillas, R., Subcritical crack propagation under cyclic and static loading in mullite and mullite-zirconia. *J. Eur. Ceram. Soc.*, 1998, **18**, 221–227.